

Photopharmacology

A Rationally Designed Azobenzene Photoswitch for DNA G-Quadruplex Regulation in Live Cells

Marta Dudek,* Lucía López-Pacios, Nasim Sabouri, Juan J. Nogueira, Lara Martinez-Fernandez, and Marco Deiana*

Abstract: G-quadruplex (G4) DNA structures are increasingly acknowledged as promising targets in cancer research, and the development of G4-specific stabilizing compounds may lay a fundamental foundation in precision medicine for cancer treatment. Here, we propose a light-responsive G4-binder for precise modulation of drug activation, providing dynamic and spatio-temporal control over G4-associated biological processes contributing to cancer cell death. We developed a specialized fluorinated azobenzene (AB) switch equipped with a quinoline unit and a positively charged carboxamide side chain, **Q-Azo4F-C**, designed for targeted binding to G4 structures within cells. Biophysical studies, combined with molecular dynamics simulations, provide insights into the unique coordination modes of the photoswitchable ligand in its *trans* and *cis* configurations when interacting with G4s. The observed variations in complexation processes between the two isomeric states in different cancer cell lines manifest in more than 25-fold reversible cytotoxic activity. Immunostaining conducted with the structure-specific G4 antibody (BG4), establishes a direct correlation between cytotoxicity and the varying extent of G4 induction regulated by the two isoforms. Finally, we demonstrate the photo-driven reversible regulation of G4 structures in lung cancer cells by **Q-Azo4F-C**. Our findings highlight the potential of light-responsive G4-binders in advancing precision cancer therapy through dynamic control of G4-mediated pathways.

Introduction

Four-stranded G-quadruplex (G4) DNA structures are intricately linked to critical biological processes, such as DNA replication, transcription, and telomere maintenance, with profound implications for cancer.^[1] Computational and experimental mapping of G4s in the human genome has revealed an enrichment of G4-forming sequences in genomic regions associated with disease states.^[2] Within the dynamic milieu of live cells, G4s emerge as significant players capable of impeding DNA transactions, acting as stable roadblocks to the replicative helicase and polymerase processivity.^[3] This unique characteristic opens a window of opportunities to introduce structure-specific DNA damage through the strategic use of tailored G4-stabilizers.^[4] G4-interacting compounds show promising therapeutic potential in synthetic lethality strategies, and are particularly effective in DNA damage response (DDR)-deficient cells, especially in combination with DNA-damaging or DDR-inhibiting drugs. G4s have also become a significant focal point in phototherapeutic approaches for cancer treatment, such as photodynamic therapy due to their unique photophysical properties such as low-energy photoionization.^[5] Their susceptibility to oxidation can indeed be harnessed in conjunction with G4-selective photosensitizers to optimize oxidative DNA damage.^[6] With regard to small molecule design, integrating light-responsive moieties into the structure of G4-binding ligands enables the remote-controlled modulation of their activity.^[7] Indeed, as an external targeting stimulus, light provides several distinct advantages, encompassing minimal toxicity, precise spatiotemporal control over drug activation by finely tuning the power, duration, and even the wavelength of the excitation source.^[8]

[*] Dr. M. Dudek, Dr. M. Deiana
Institute of Advanced Materials, Faculty of Chemistry
Wrocław University of Science and Technology
Wyb. Wyspiańskiego 27, 50-370 Wrocław (Poland)
E-mail: marta.ziemianek-dudek@pwr.edu.pl
m.deiana@pwr.edu.pl

L. López-Pacios, Dr. J. J. Nogueira
Departamento de Química, Facultad de Ciencias
Universidad Autónoma de Madrid, Campus de Excelencia UAM-
CSIC
Cantoblanco, 28049 Madrid (Spain)
Prof. Dr. N. Sabouri, Dr. M. Deiana
Department of Medical Biochemistry and Biophysics
Umeå University
SE-901 87 Umeå (Sweden)

Dr. J. J. Nogueira
Institute for Advanced Research in Chemistry (IAdChem)
Universidad Autónoma de Madrid, Campus de Excelencia UAM-
CSIC
Cantoblanco, 28049 Madrid (Spain)

Dr. L. Martinez-Fernandez
Departamento de Química Física de Materiales, Instituto de
Química Física Blas Cabrera, CSIC
28006, Madrid (Spain)

© 2024 The Authors. Angewandte Chemie International Edition published by Wiley-VCH GmbH. This is an open access article under the terms of the Creative Commons Attribution License, which permits use, distribution and reproduction in any medium, provided the original work is properly cited.

In this context, the Balasubramanian lab reported the use of a caged derivative of the renowned G4-stabilizing compound pyridostatin (PDS) to regulate the transcription of G4-containing genes.^[9] Vilar's group has developed a rotaxane incorporating a square planar Pt^{II}-salphen complex with photon-dependent G4-binding activity.^[10] Recently, we investigated the photoinduced macrocyclization of a helicenoid quinoline derivative of binaphthol, resulting in a π -extended dicationic compound.^[7g] The latter demonstrated the capacity to stall DNA polymerase by selectively stabilizing G4 structures linked to oncogenic promoters and telomere repeat units. In a series of papers, the Galan lab explored the G4-interacting binding properties of a photo-responsive stiff-stilbene ligand using both experimental and computational approaches.^[11] While these studies have demonstrated some degree of success, their limitations, such as the requirement for UV light (≤ 365 nm) to excite the ligand's active form and/or the absence of a reversible process, make them far from ideal for usage in cells. Molecular switches, incorporating the versatile azobenzene (AB) unit,^[7e] offer a promising avenue to overcome the existing limitations. In this context, the pioneering work of Zhou's group opened up new possibilities for regulating G4 structures derived from telomeric sequences using AB switches decorated with quaternary ammonium groups, including aliphatic and aromatic species.^[7b,c,e,12] The authors demonstrated robust G4 folding-unfolding activity associated with the isomeric states of the photochrome between the *trans* and *cis* configurations.^[7b,c,e] The same group further applied this principle to manipulate enzymatic reactions, demonstrating the potential to regulate thrombin activity by modulating the conformation of a DNA-based inhibitor system.^[7e,12] This system consists of a central telomeric G4-forming sequence acting as a regulatory element fused with two thrombin-binding aptamers that cooperatively prevent fibrinogen from binding to thrombin. Depending on either the geometric state of the photoswitch^[7e] or host-guest supramolecular interactions with a macro-cavitant,^[12] the telomeric G4-acting element could fold or unfold, providing reversible control over the thrombin-fibrinogen reaction. However, up to now, these studies have relied on UV light to induce *trans*-to-*cis* isomerization and have been limited to test-tube settings, not yet demonstrating their full potential in biological systems, such as cell studies. AB functionalized with *ortho*-fluorine atoms has a lower energy of the *n*-orbital of the *cis*-isomer, resulting in a separation of the *trans* and *cis* isomer' $n \rightarrow \pi^*$ absorption bands, corresponding to absorption to the S₁ electronic state.^[13] This provides switching possibilities with visible light, avoiding the need for UV irradiation. Recently, we demonstrated that these types of fluorinated ABs could target G4s, with the recognition process and optical output modulated by changing the isomeric states of the switch using only visible light.^[7f] However, these results were again limited to test-tube settings. Consequently, we decided to investigate the potential of this class of photochromes in live cell studies. In this work, we developed an *ortho*-fluorinated AB switch with nearly quantitative two-way isomerization using visible light, making it suitable for live cell applications. This

compound (**Q-Azo4F-C**, Figure 1A), equipped with a quinoline unit on one side and a positively charged carboxamide side chain on the other, is designed to enhance both its G4-interacting binding properties and its uptake in cancer cells. The *trans* and *cis* forms of **Q-Azo4F-C** exhibit distinct coordination modes associated with the isomerization process. Biophysical studies, molecular dynamics (MD) simulations, and G4 immunodetection techniques in cancer cells show that the *cis* isomer promotes G4 formation through external binding. In contrast, the *trans* isomer partially unfolds G4s by intercalating into the central guanine (G)-tetrad. The ability to fold and unfold G4s correlates positively with the cytotoxic effects of the *trans* and *cis* isomers, respectively, across various cancer cell lines. Moreover, the compound enables in-cell photoregulation of G4s, which is achieved by converting the G4-forming and cytotoxic *cis* isomer into a non-toxic, non-G4-forming *trans* state.

Results and Discussion

Design and Photochemical Characterization of the Molecular Switch

Q-Azo4F-C compound consists of a quinoline unit and a positively charged carboxamide side chain, directly linked to the *para* position of the AB core. This synthetic approach aims to functionalize the molecule with two flexible scaffolds, each potentially influencing the G4 in a complementary or opposing manner, depending on the switch's geometric configuration. In fact, while the quinoline moiety, exemplified by PhenDC3^[14] and PDS,^[15] is known for stabilizing G4 structures, positively charged amino groups^[16] can destabilize/unfold G4s. Building on this knowledge, **Q-Azo4F-C** (Figure 1A) was synthesized in nine steps, including a bromination/cyanation/hydrolysis/esterification/oxidative coupling/hydrolysis/ followed by two final amide coupling reactions and deprotection of the amine groups (see Supporting Information pp. S6–S9 for details concerning synthesis). The UV/Vis spectrum of **Q-Azo4F-C** in the *trans* state exhibited a prominent $\pi \rightarrow \pi^*$ absorption peak at 335 nm and a less intense $n \rightarrow \pi^*$ band around 472 nm (Figure 1B). Exposure to visible light ($\lambda \geq 550$ nm) induces *trans*-to-*cis* isomerization, leading to a reduction in the $\pi \rightarrow \pi^*$ band and an increase in the $n \rightarrow \pi^*$ absorption, coinciding with a notable blue-shift (~ 425 nm) of approximately 50 nm. The distinction in the $n \rightarrow \pi^*$ bands between the two isomers facilitates the isomerization of the switch using visible light in both directions. This process generates photostationary states (PSSs) comprising 93 % *cis* isomer when exposed to green light ($\lambda \geq 550$ nm) and 92 % *trans* isomer under blue light (436 nm), as quantitatively determined by ¹H and ¹⁹F nuclear magnetic resonance (NMR) spectra analysis (Figures 1C, S5 and S6). Notably, **Q-Azo4F-C** in the *cis* form exhibited high thermal stability (Figure 1D, Supporting Information pp. S11), boasting a half-life of approximately 62 days at 25 °C, indicative of an activation

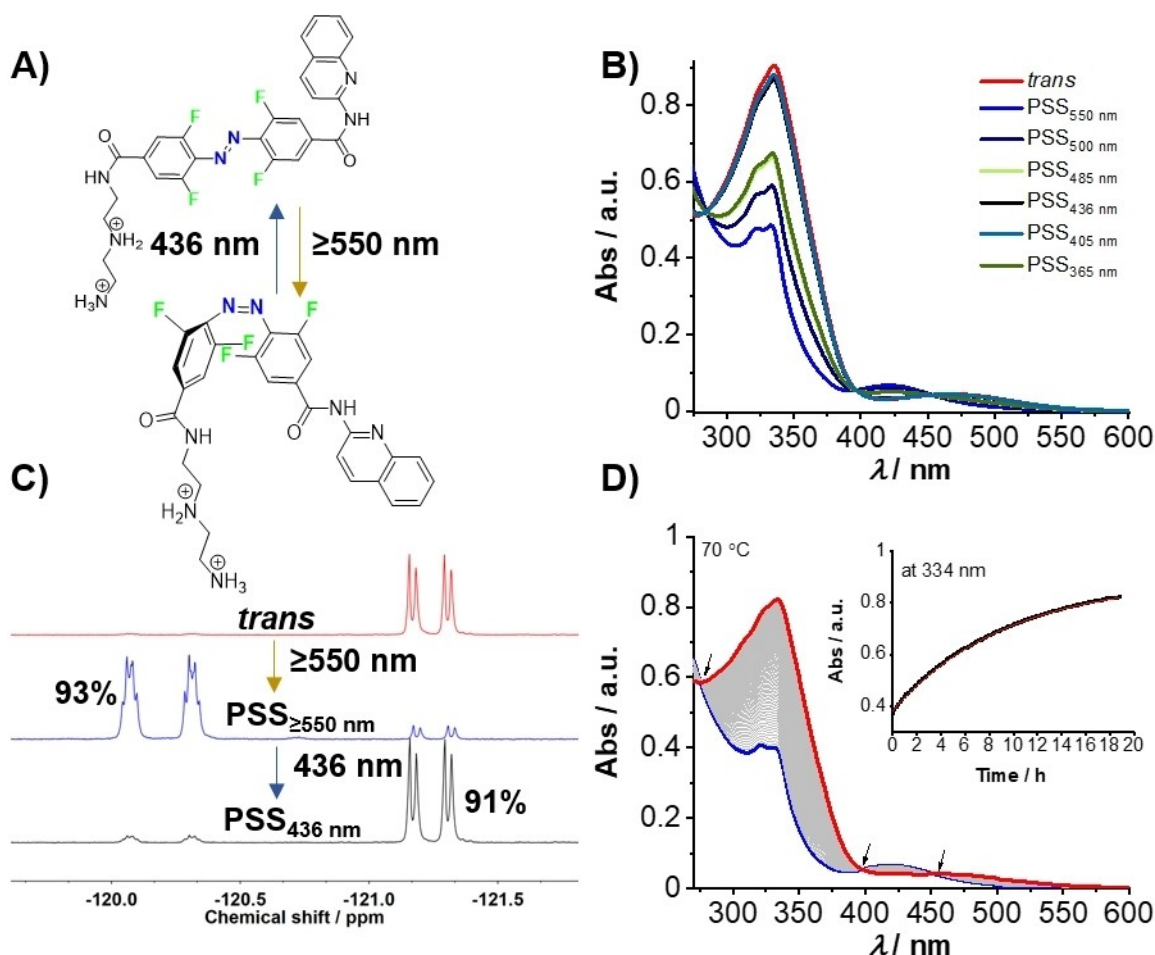


Figure 1. (A) Chemical structures of **Q-Azo4F-C** in *trans* or *cis* forms. (B) Absorption spectra of **Q-Azo4F-C** recorded in DMSO solution under excitation with light of different wavelengths ($c_{\text{Q-Azo4F-C}} = 30 \mu\text{M}$). (C) Quantification of the PSSs of **Q-Azo4F-C** ($c_{\text{Q-Azo4F-C}} = 3 \text{ mM}$, in methanol- d_4 at 25 °C) by ^{19}F NMR spectroscopy. The contents of *trans* and *cis* isomers in solution were calculated from the intensity ratios of the integrals of the corresponding peaks. (D) UV/Vis absorption spectra for 30 μM solution of **Q-Azo4F-C** at 70 °C in DMSO in the PSS after ≥ 550 nm irradiation (blue curve), and spectral evolution during the *cis-trans* thermal return. The inset presents absorption changes monitored at 334 nm during *cis-trans* thermal relaxation.

barrier of 102 kJ/mol, as estimated by the Arrhenius equation (Table S1).

Photoregulation of G4-Associated Binding Mechanisms

The binding affinity of **Q-Azo4F-C** for G4s in either *trans* or *cis* configurations (Table S2) was quantified using a fluorescence quenching assay (Figure 2A). This assessment involved monitoring the change in fluorescence intensity induced by **Q-Azo4F-C** on a Cyanine 5 (Cy5)-labeled G4 oligonucleotide (*c-MYC* Pu22) derived from the promoter region of the cancer-associated *MYC* gene (Figure 2A).^[17] Nonlinear curve-fitting procedures, based on fluorescence quenching mediated by proximal ligand binding at the 5'-G-tetrad end, were applied to both isomers. These procedures demonstrated robust binding strengths to the G4 template, with association constants of $2.5 \times 10^6 \text{ M}^{-1}$ for the *trans* isomer and $3.5 \times 10^5 \text{ M}^{-1}$ for the *cis*-rich mixture. These findings were further corroborated by microscale thermophoresis

(MST) experiments using the natural G4-forming sequence found in the promoter region of hypoxia-inducible factor 1 alpha (*HIF-1a*), a master regulator in the pathogenesis of cancer.^[18] These experiments provided association constants of $1.0 \times 10^6 \text{ M}^{-1}$ for the *trans* isomer and $8.4 \times 10^4 \text{ M}^{-1}$ for the *cis*-rich mixture (Figure S8). The difference in binding strength can be attributed to the distinct degrees of planarity exhibited by these two isomeric forms. The structure of the *trans* form, indeed, facilitates easier establishment of π -stacking interactions with the G-tetrads. Conversely, the distorted configuration of the *cis* form partially impedes π -stacking interactions resulting in a coordination mode that likely engages the G-tetrads only partially, primarily relying on groove-binding and electrostatic attractions. As discussed later, this fact is corroborated by the computational simulations. To gain a more comprehensive insight into the structural basis of the interaction between **Q-Azo4F-C** and G4s, ^1H NMR experiments were conducted (Figures S9–S15) by using the well-characterized telomeric G4 sequences Tel22- Na^+ (Figures S10–S12) and Tel23- K^+ (Figures S13–

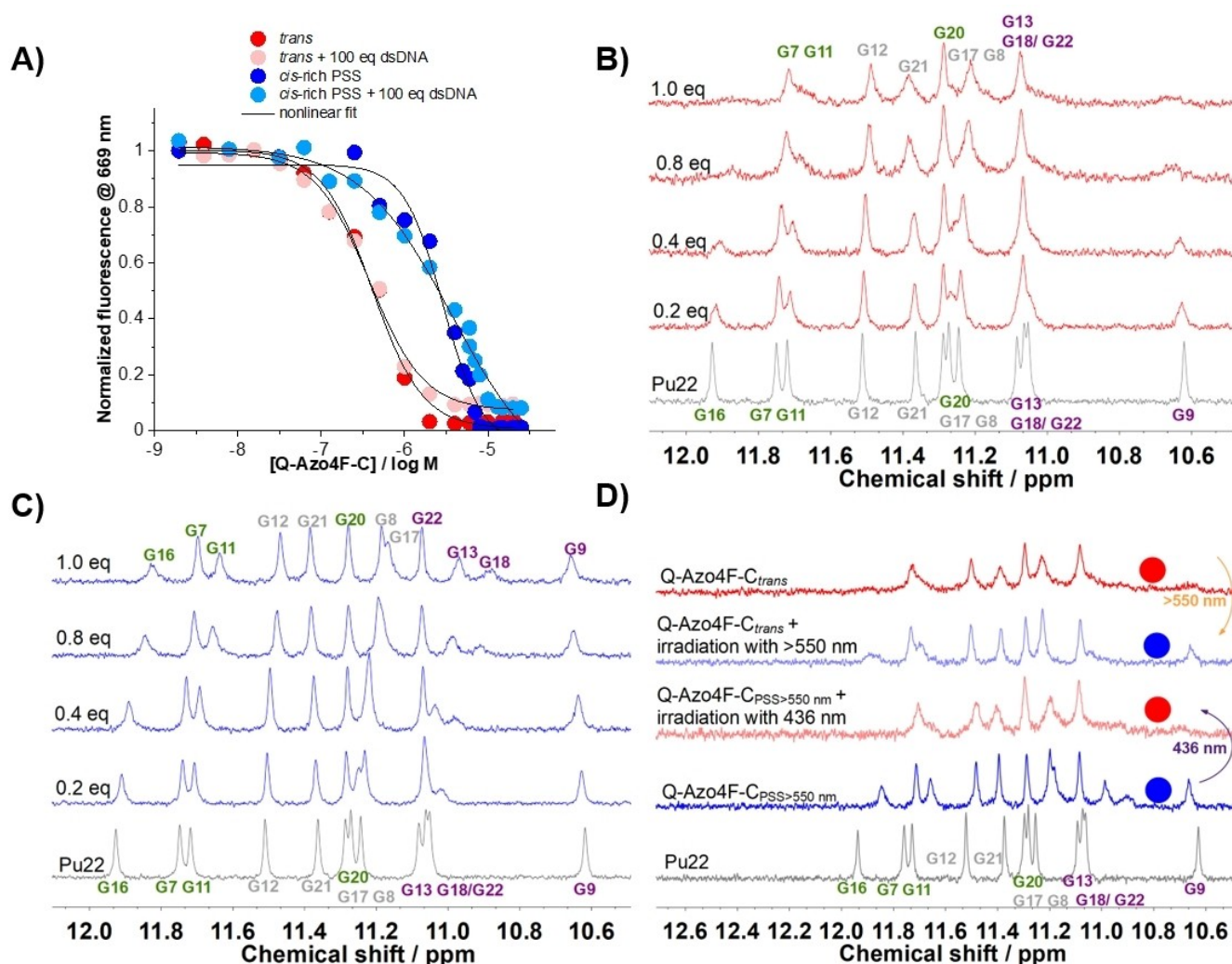


Figure 2. Biophysical data demonstrate the interaction between **Q-Azo4F-C** and G4s. (A) Fluorescence changes of Cy5-*c-MYC* Pu22 G4 ($c_{G4} = 50$ nM, 50 mM Tris pH 7.2, 100 mM KCl) in the presence of the incremental addition of **Q-Azo4F-C** in either *trans* (red dots) or *cis*-rich PSS (blue dots). The competitive assay was performed in the presence of 100 eq. of dsDNA for *trans* (pink dots) or *cis*-PSS (pale blue dots). (B–C) ^1H NMR spectra of the G-tetrad imino protons in the absence (0.0 eq) or presence (0.2, 0.4, 0.8, and 1.0 eq) of **Q-Azo4F-C** *trans* (B) and of **Q-Azo4F-C** *cis*-rich mixture (C). (D) ^1H NMR spectra of *c-MYC* Pu22 alone (grey), *c-MYC* Pu22 with 1.0 eq of **Q-Azo4F-C** *trans* (red) or **Q-Azo4F-C** *cis*-rich mixture (blue). ^1H NMR spectra representing in situ photoswitching were taken after irradiation with 436 nm (*cis*-to-*trans* isomerization, pink), and clearly show the change in imino protons shift, or after irradiation with ≥ 550 nm (*trans*-to-*cis* isomerization, light blue), and show minor change in imino protons shift. The red and blue circles are provided to aid in data interpretation, highlighting which spectra should align if the system achieves full reversibility.

S15) as well as *c-MYC* Pu22 (Figures 2B–D and S9).^[17,19] In its unbound state, *c-MYC* Pu22 displayed 12 imino proton peaks, with their assignments having been reported previously.^[19c] Addition of **Q-Azo4F-C** in its *trans* configuration induced a chemical shift alteration in almost all imino protons associated with the terminal G-tetrad ends, along with certain ones connected to the central G-tetrad (Figure 2B). Specifically, our findings revealed that **Q-Azo4F-C** significantly impacted G16, G11, and G20, along with G9, G13, and G18 linked to the 5'- and 3'-ends, respectively. Additionally, it affected G21 and G17 associated with the central G-tetrad. Notably, a progressive broadening of the imino signals was observed during the titration, resulting in the detection of only 6 out of the initial

12 imino protons at equimolar concentrations of **Q-Azo4F-C** and *c-MYC* Pu22. These observations suggest the potential for the *trans* form to coordinate the *c-MYC* Pu22 template through not only the two G-tetrad ends but also the central G-quartet. A comparison of these findings with recently reported NMR data for photochromic compounds interacting with G4s hints at the possibility that the *trans* isomer might have induced a partial unfolding or opening of the G4 structure via an unconventional intercalative binding mechanism.^[11b] Interestingly, ^1H NMR experiments performed with Tel23- K^+ and **Q-Azo4F-C** in *trans* configuration show not only broadening and annulation of specific resonances but also the appearance of new signals, which may be attributed to the eventual emergence of misfolded

states, as previously reported (Figure S13).^[11b] Similar experiments carried out with the *c-MYC* Pu22 titrated with the *cis*-rich mixture of **Q-Azo4F-C** showed minimal impact on the guanines linked to the 5'-end (Figure 2C). However, it notably affected G13 and G18 associated with the 3'-end, as well as G17 linked with the central G-tetrad. Additionally, all 12 imino proton peaks attributed to *c-MYC* Pu22 remained distinct at the conclusion of the titration involving the *cis*-rich mixture. These data suggest that the binding of the *cis* form to the *c-MYC* Pu22 template likely involved the 3'-end, resulting in minimal perturbation of the G4 structure. It is noteworthy that the *cis*-to-*trans* isomerization, triggered by light, causes the broadening of imino proton signals together with attenuation of G9 and G16 resonances particularly observed in the *trans-c-MYC* Pu22 system (Figure 2D). However, the reversal of *trans*-to-*cis* isomerization did not undo the alterations associated with the *cis-c-MYC* Pu22 complexation process. This is likely due to the *trans* isomer's tendency to remain firmly bound within the G4 intercalation site, consistent with its high binding strength. Overall, these findings indicate a significant level of reversibility in the process, albeit not easily attainable bidirectionally.

To further explore the binding modes and to compute the interaction free energies of **Q-Azo4F-C** to *c-MYC* Pu22, we conducted molecular docking and classical molecular dynamics (MD) simulations. During the first docking

studies, using as target receptor the *c-MYC* Pu22 structure resolved by NMR (PDB code 1XAV.pdb^[20]), two main external poses, based on their abundance, were obtained for both *cis* and *trans* forms (Figure 3A and B). Aiming to investigate the intercalated possibility, the *c-MYC* Pu22 structure was opened through a combination of MD and umbrella sampling techniques (see pp. S26–S27 of the SI). After equilibration of the final opened structure, new docking calculations provided the most populated internal intercalated *cis* and *trans* poses (Figure 3A and B). Then, for the three docking poses (two external and one internal), MD simulations combined with free-energy calculations (see pp. S37–S38 of the SI) were run to calculate the binding free energies of the *cis* and *trans* isomers and to decompose the energy into the contributions from the different nucleobases. By comparison of the most stable pose of each isomer (Table S11), the *trans* state interacts in a stronger way (−106.6 kcal/mol) than the molecule in the *cis* state (−94.8 kcal/mol), in qualitative agreement with the association constants determined by the MST measurements. For the *trans* isomer, the intercalative pose is energetically favored over the two external poses. The energy decomposition analysis shown in Figure 3C reveals that the intercalative binding is dominated by the interaction with the three tetrads (186.6 kcal/mol), while the interaction with the external nucleobases is less than half in magnitude (82.3 kcal/mol). In a more specific way, the intercalative

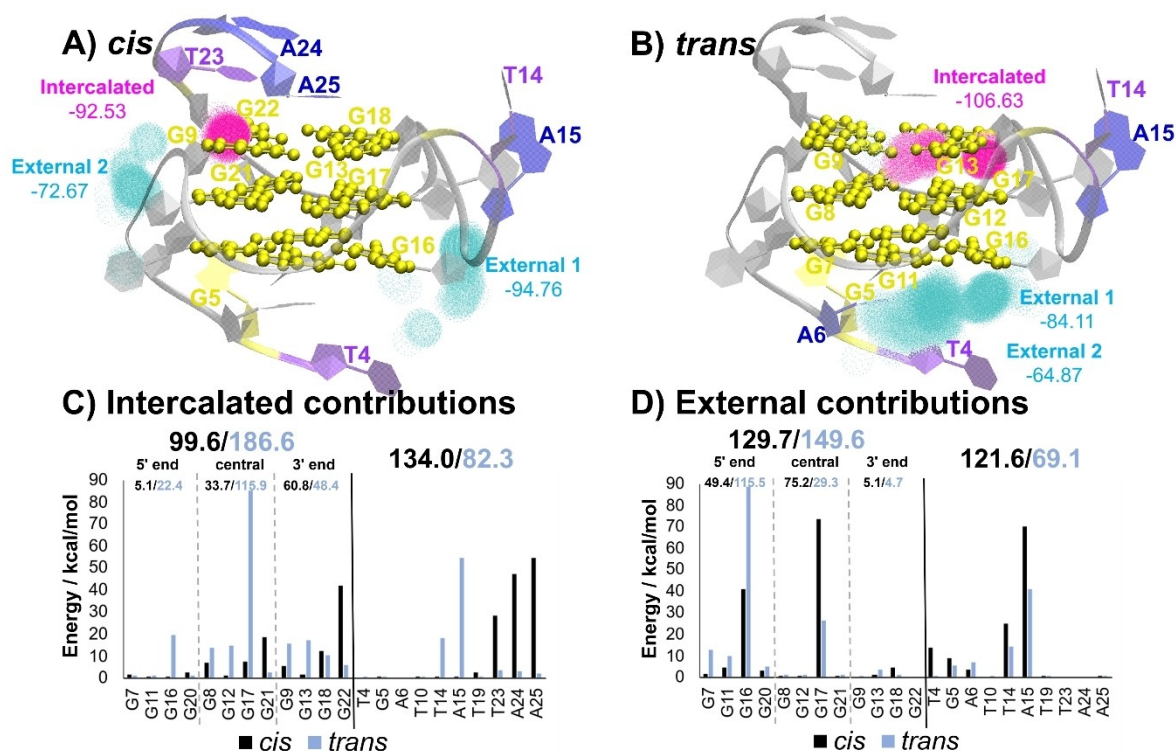


Figure 3. Schematic representation of the most probable *cis* (A) and *trans* (B) poses obtained during the docking studies together with the binding energies from subsequent MD simulations. The densities of the point clouds indicate the occurrence of the different binding poses. Per-nucleobase energy decomposition analysis for the intercalated (C) and the most favourable external (D) poses. The numbers above the bars indicate the contribution from the external and tetrad nucleobases. In turn, the last one is split into contributions from the central and 5'- and 3'-end tetrads for the *cis* and *trans* isomers.

binding of the *trans* isomer is controlled by the interaction with the central tetrad (115.9 kcal/mol), especially with G17, although the interactions with the 5'- and 3'-end ones are not negligible, again in consonance with the shifts observed in the NMR experiments. On the contrary, for the *cis* isomer, the external and intercalative poses will co-exist, in the case that both are kinetically favored, although with a slight predominance of the external one, which is 2 kcal/mol more stable. In this case, as displayed in Figure 3D, the interaction between the *cis* structure and G4 in the external pose has similar contributions from the external nucleobases (121.6 kcal/mol) and from the ones forming the three tetrads (129.7 kcal/mol). As mentioned above, the NMR data suggest that the binding of the *trans* isomer might have induced a partial unfolding of the G4, while the binding of the *cis* isomer resulted likely in only a small structural perturbation. This hypothesis is corroborated by the MD simulations, where the G4 structure is better preserved along the dynamics for the external pose of the *cis* isomer than for intercalated *trans* isomer (see Figures S45 and S61 of SI).

The structural data obtained for **Q-Azo4F-C** complexed with various G4 structures prompted us to further investigate G4 regulation using complementary biophysical methods. Circular dichroism (CD) titration experiments, performed on parallel (*HIF-1 α* , *c-MYC* Pu22 and *c-MYC* Pu24), hybrid (Tel-22 in K⁺), and antiparallel (TBA and Bom17) G4 structures, revealed that the *trans* isomer induced pronounced spectral changes, especially in hybrid and antiparallel G4 topologies, indicative of a G4 unfolding binding event (Figures S16–S17). In contrast, the *cis*-rich mixture exhibited minimal spectral changes to these G4 structures compared to the *trans* isomer (Figures S16–S17). It is likely that the changes observed for the *cis*-rich mixture may be partially attributed to the residual *trans* isomer present in the solution (~10 %) after photoconversion. Interestingly, almost no or very weak changes were detected for **Q-Azo4F-C** bound to duplex DNA in either configuration, providing initial evidence of a degree of selectivity for G4s over duplex DNA (Figure S18). To further investigate the roles of the *trans* and *cis* isomers in controlling the folding and unfolding states of G4s, we conducted CD-based thermal melting assays, measuring molar ellipticity as a function of increasing temperature. The melting temperatures (ΔT_m) indicated a higher degree of G4 stabilization in the presence of the *cis*-rich mixture of **Q-Azo4F-C** compared to the *trans* form, while both isomers displayed a negligible effect on duplex melting temperature (Figure 4A). Overall, the CD data clearly support the potential folding-unfolding event mediated by the photochrome and demonstrate selectivity for G4 over duplex DNA. This selectivity was further investigated through competitive fluorescence titration experiments to test the binding selectivity of G4 ligands. These experiments employed a large excess of 100 equivalents of duplex DNA compared to the G4 concentration. As depicted in Figure 2A, the presence of dsDNA did not affect the binding affinity of the *trans* and *cis*-rich mixtures of **Q-Azo4F-C**, indicating a higher binding affinity for G4 DNA over dsDNA. To rule out any potential

interference from duplex DNA on the coordination mode of the photochrome to G4s, we conducted ¹H NMR competitive binding experiments using *c-MYC* Pu22 as a G4 model template. The detected chemical shift perturbations of the imino protons in the **Q-Azo4F-C** (*trans* or *cis*-rich PSS)-G4 complexes were unaffected by duplex DNA, confirming the ligand's higher affinity for G4 structures and demonstrating that isomeric states can precisely trigger conformational changes in the G4 template despite the presence of duplex DNA (Figures 4B and S19).

The complex intracellular milieu contains various metal ions that can promote conformational alterations in G4 structures, potentially affecting or hindering ligand binding.^[7b,c] To address this, we investigated the role of the most abundant cellular ions (K⁺, Na⁺, Mg²⁺, and Ca²⁺),^[21] both individually and in combination, on the recognition ability of **Q-Azo4F-C** toward the *c-MYC* Pu22 template. As depicted in Figure 4C–D and Supplementary Figures S20–S25, the presence of these different ions did not cause significant changes in the coordination mode of the photochrome to *c-MYC* Pu22. These findings further support the potential of **Q-Azo4F-C** for translation into live cell experiments.

Visible Light Modulation of Cytotoxicity and G-Quadruplex Folding/Unfolding in Cancer Cells

The almost complete two-way isomerization and the ability to alter **Q-Azo4F-C**'s binding mode on G4 structures using visible light led us to explore regulating cytotoxicity through the switch's state interconversion (Figures 5 and S26). For this purpose, four different human cancer cell lines originating from various tumors were utilized, including cervical cancer HeLa cells, osteosarcoma U2OS cells, breast cancer MCF-7 cells, and lung adenocarcinoma A549 cells. In its *trans* configuration, **Q-Azo4F-C** exhibited mild cytotoxic effects, displaying varying half-maximum inhibitory concentrations (IC₅₀) across different cell lines: IC_{50(trans)} (U2OS) = 41.1 ± 10.0 μM, IC_{50(trans)} (HeLa) = 40.4 ± 5.7 μM, IC_{50(trans)} (MCF-7) > 100 μM, and IC_{50(trans)} (A549) > 100 μM. Conversely, the *cis*-rich PSS, **Q-Azo4F-C** demonstrated heightened cytotoxicity with IC_{50(cis-rich PSS)} (U2OS) = 3.7 ± 0.8 μM, IC_{50(cis-rich PSS)} (HeLa) = 2.6 ± 0.2 μM, IC_{50(cis-rich PSS)} (MCF-7) = 4.0 ± 0.5 μM, and IC_{50(cis-rich PSS)} (A549) = 4.8 ± 0.2 μM. These findings yielded high *trans* IC₅₀/*cis*-rich PSS IC₅₀ ratios ranging from 11 to >25, indicating the potential to modulate cytotoxicity through the application of visible light. To examine this hypothesis, we exposed the cells to cytotoxic levels of **Q-Azo4F-C** in its *cis*-rich PSS for 1 hour. Subsequently, the cells underwent a 10-minute exposure to blue light at 436 nm to induce the *cis*-to-*trans* isomerization. In this scenario, we observed a viability recovery of approximately 40 % in U2OS, 50 % in MCF-7, 70 % in HeLa, and complete restoration (100 %) in A549 cells (Figure 5).

We then examined whether the light-dependent cytotoxicity displayed by the *trans* and *cis* isomers correlates with their ability to fold G4s inside cells (Figure 6). For this

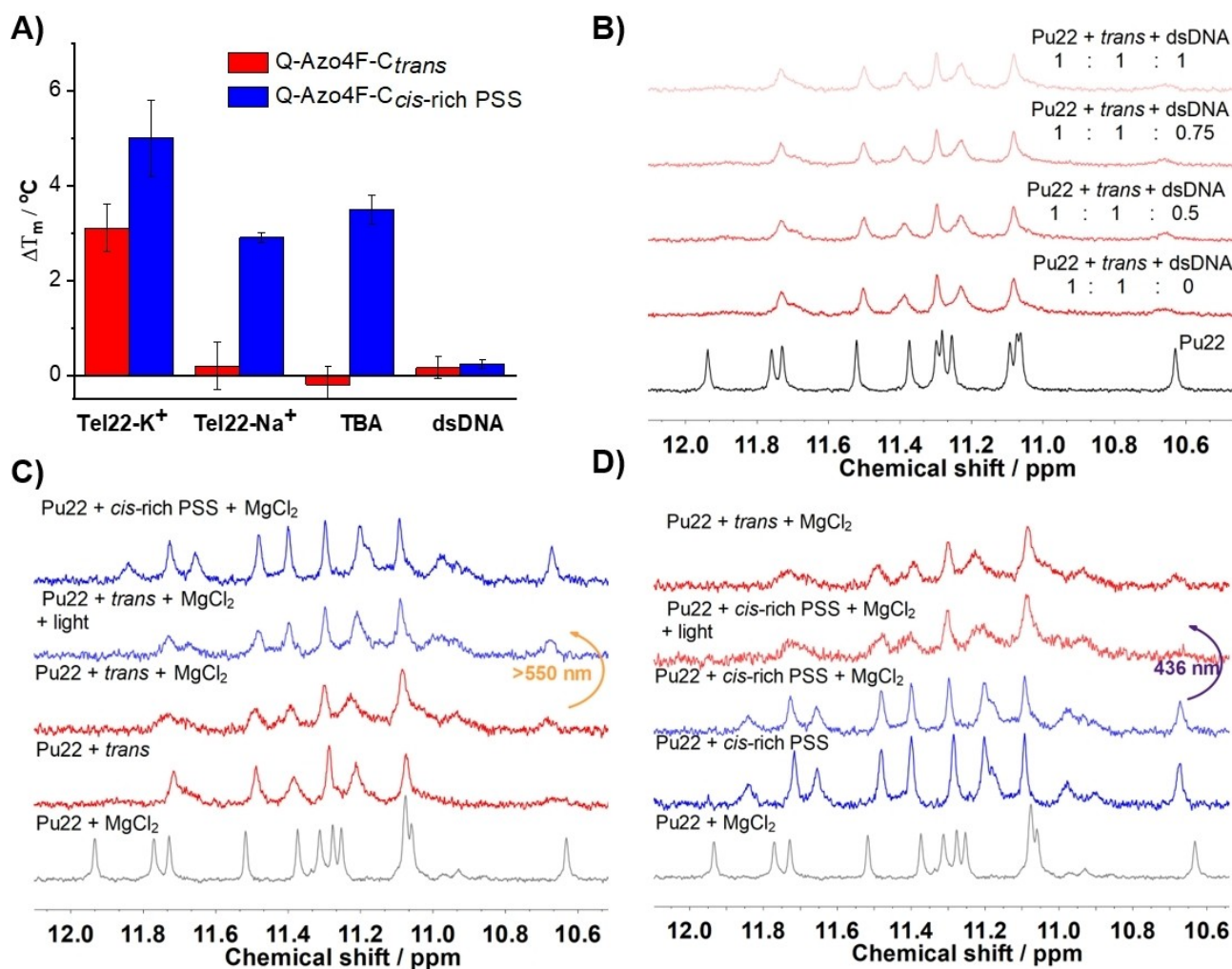


Figure 4. (A) Thermal stabilization analysis of Q-Azo4F-C *trans* and *cis*-rich PSS ($c_{\text{Q-Azo4F-C}} = 8 \mu\text{M}$) on Tel22- K^+ , Tel22- Na^+ , TBA, and dsDNA ($c_{\text{G4/duplex}} = 2 \mu\text{M}$). Tris-HCl buffer = 10 mM, KCl = 5 mM for Tel22- K^+ , TBA, dsDNA, and NaCl = 15 mM for Tel22- Na^+ . Results are presented as an average of three independent experiments, the error bars indicate SD. (B) ^1H NMR spectra highlighting the G-tetrad imino protons of *c*-MYC Pu22 (black line, bottom) interacting with Q-Azo4F-C in *trans* form (red line) at different G4 to duplex DNA ratios. (C, D) ^1H NMR spectra highlighting the G-tetrad imino protons of *c*-MYC Pu22 ($c_{\text{KCl}} = 33 \text{ mM}$) interacting with 1 eq. of Q-Azo4F-C in its *trans* (C) or *cis*-rich PSS (D) forms, in the presence of 1 mM MgCl_2 . For comparison, the ^1H NMR spectra of Q-Azo4F-C in either *trans* or *cis*-rich PSS forms bound to *c*-MYC Pu22 in the presence of 33 mM KCl but in the absence of MgCl_2 are also shown. The spectra, representing both the binding process and in situ photoswitching, indicate that MgCl_2 has no influence on the binding of the ligand to the G4 structure.

purpose, we selected A549 cells as a model system, as the *trans* form of Q-Azo4F-C demonstrated minimal cytotoxicity, while the *cis* form exhibited substantial cytotoxicity, providing a wide therapeutic window. To visualize and quantitatively determine the G4 levels in A549 cells, we utilized the extensively characterized G4-specific antibody BG4.^[2a,b] BG4 demonstrates a robust affinity for G4 structures across a spectrum of topologies and molecularities, with binding constants in the low nanomolar range.^[2b] This strong binding affinity ensures minimal competition with Q-Azo4F-C for G4 structures, as the latter exhibits a significantly lower binding affinity, thereby facilitating its easy displacement from these structures. Furthermore, BG4's ability to bind to both fully folded and partially folded G4 structures, coupled with its inability to interact with unfolded G4s, provides a reliable method to assess the

effects of the isomeric forms of the switch on G4 structures within a cellular context.^[2b] In these experiments, cells were exposed to different concentrations (6, 7, and $8 \mu\text{M}$) of Q-Azo4F-C in either *trans* form or *cis*-rich mixture, after which immunofluorescence (IF) analyses were conducted. The chosen concentrations of Q-Azo4F-C in its *cis*-rich PSS were slightly higher than the previously calculated IC_{50} value of $\sim 5 \mu\text{M}$ obtained in cell viability experiments. However, in the IF experiments, significantly different seeding densities were employed—approximately 100,000 cells per dish compared to 5,000 cells per well in cytotoxic studies, known to influence a drug's sensitivity.^[22] Nevertheless, under the conditions of the IF experiment, the analyzed cells were confirmed to be viable. Compared to mock-treated cells, cells treated with Q-Azo4F-C_{*trans*}, displayed a decreased number of BG4 foci (Figure 6B, C), suggesting an unfolding

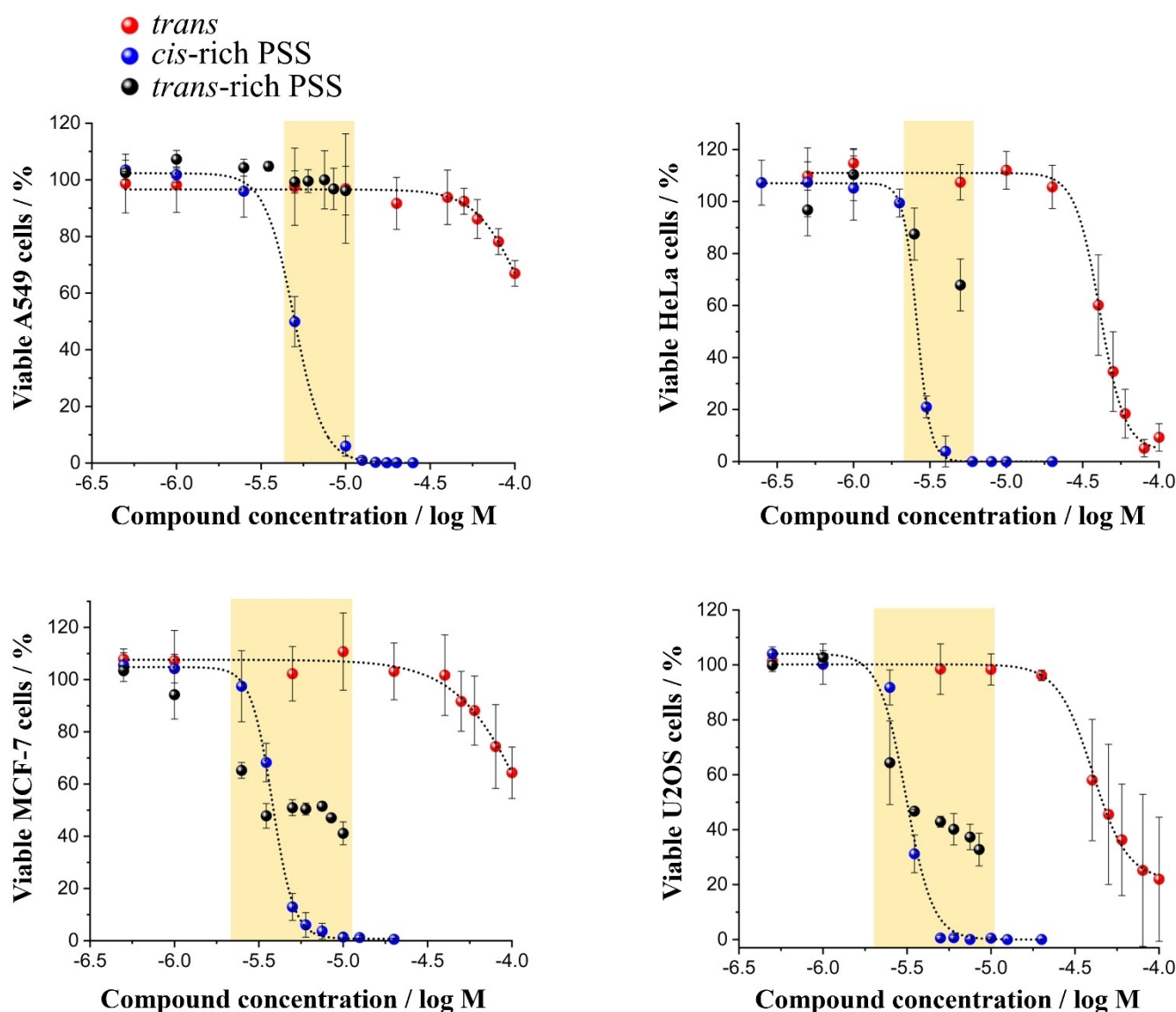


Figure 5. Antiproliferative activity of **Q-Azo4F-C** on various cancer cell lines (A549, HeLa, MCF-7, and U2OS) using both *trans* and *cis*-rich PSS, followed by evaluation post-photoconversion into the *trans*-rich PSS. The in-cell *cis*-to-*trans* isomerization was achieved by incubating the *cis*-rich PSS for 1 hour followed by exposing the cells to 10 minutes of 436 nm blue light irradiation. The yellow bars illustrate the transformation of cytotoxic *cis*-rich PSS doses into less or even non-toxic *trans*-rich PSS concentrations. Error bars indicate mean \pm SD ($n = 3$).

effect on G4 structures. Specifically, the *trans* isomer demonstrated a concentration-dependent impact on G4s, leading to reductions of approximately 0.7-fold, 0.6-fold, and 0.3-fold in the levels of nuclear BG4 foci at concentrations of 6, 7, and 8 μ M, respectively. Conversely, the photo-induced *cis*-rich PSS of **Q-Azo4F-C** led to increased levels of nuclear BG4 foci, resulting in enhancements of about 2.1-fold, 10.1-fold, and 5.6-fold at concentrations of 6, 7, and 8 μ M, respectively. These findings suggest that the development of G4-binders should not focus exclusively on enhancing the binding affinity of compounds to G4 structures. Instead, it is crucial to prioritize the addition of substituents and structural modifications that enable diverse coordination modes. Although the *trans* isomer exhibits a higher affinity for G4 structures and was expected to aid in G4

folding, its atypical binding mechanism—likely involving partial intercalation into the G4 cavity—actually unfolds/opens the G4 architecture, leading to reduced BG4 signal. On the other hand, the *cis* form, despite its lower affinity for G4 binding, maintains the integrity of G4 structures due to its non-disruptive coordination mode. This allows it to effectively fold G4 structures within cells without significantly altering the G4 framework.

If, on one hand, G4 stabilization can serve as a strategic means to cause substantial damage to the genome of cancer cells, an overabundance of G4s resulting from impaired G4-helicase function or the presence of G4-stabilizing ligands can contribute to various age-related disorders, such as certain neurodegenerative conditions (e.g., amyotrophic lateral sclerosis (ALS) and frontotemporal dementia

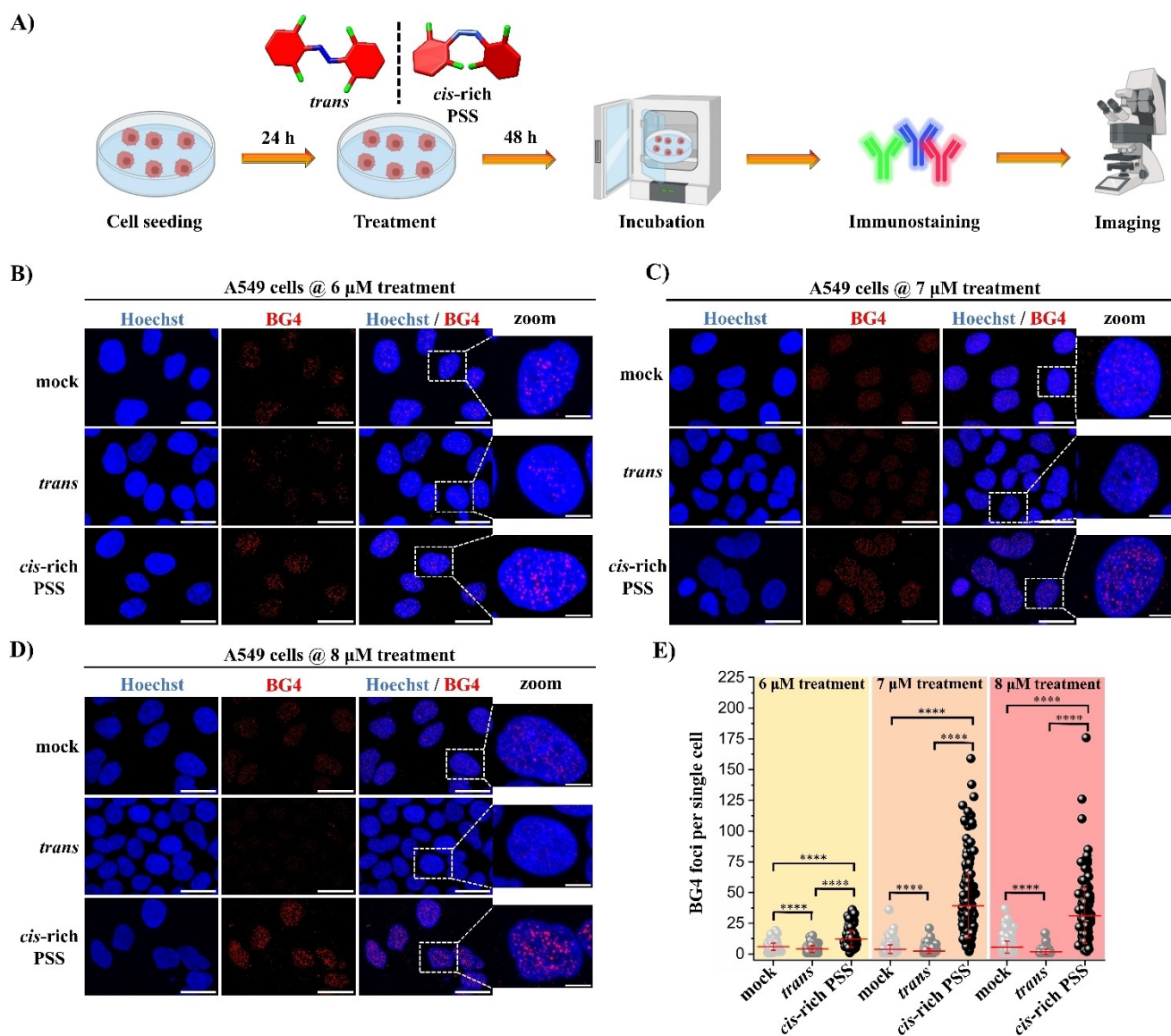


Figure 6. G4 visualization in A549 cells utilizing the G4-specific antibody BG4. (A) A schematic illustration delineating the workflow for G4 immunodetection within cells. The cells were exposed to various concentrations of **Q-Azo4F-C** in either *trans* or *cis*-rich PSS forms prior to BG4 immunostaining and imaging. Image created with Biorender.com (B–D) Immunofluorescence staining of A549 cells treated with differing concentrations (6, 7, and 8 μ M) of **Q-Azo4F-C** in *trans* or *cis*-rich PSS, or with equivalent amounts of DMSO. A549 cells were co-stained with the nuclear dye Hoechst 33342 (500 nM, blue). Red foci indicate BG4-mediated G4 recognition. $\lambda_{exc}/\lambda_{em}$: 405/420–460 nm for Hoechst (blue signal) and 598/620–750 for BG4 (red signal). The scale bar is set at 20 μ m for regular images and 5 μ m for the enlarged images. (E) Quantification of BG4 signal in the nucleus of A549 cells in the experimental conditions provided in B–D. Data represent populations of individual cells (for the 6 μ M system: $N_{mock}=201$ cells, $N_{trans}=164$ cells, $N_{cis-rich PSS}=153$ cells; for the 7 μ M system: $N_{mock}=279$ cells, $N_{trans}=341$ cells, $N_{cis-rich PSS}=232$ cells; for the 8 μ M system: $N_{mock}=277$ cells, $N_{trans}=131$ cells, $N_{cis-rich PSS}=176$ cells). The error bars represent mean \pm SD. Data analysis was performed using a two-sample *t*-test, and the significance level is denoted by the asterisks (**** $p < 0.0001$).

(FTD)), and specific genetic disorders associated with premature aging (e.g., Werner syndrome).^[23] Hence, special caution must be exercised regarding the use of G4 ligands within the realm of tumor biology, as they could accumulate and potentially damage neurons.^[24] Consequently, the regulation of G4-folding and unfolding using a singular molecular tool holds promise for interventions aimed at both inhibiting or enhancing DNA repair efficiency. To explore the potential of controlling G4 formation within cells using light, we conducted in-cell photomodulation experiments

(Figure 7). As anticipated, using the *cis*-rich PSS of **Q-Azo4F-C** at a concentration of 7 μ M resulted in an 8.8-fold increase in nuclear BG4 foci, while the *trans* form decreased the number of G4 foci by 0.5-fold. Interestingly, the photomodulation achieved by incubating the *cis*-rich PSS in the cell for 1 hour and exposing the cell solution to 10 minutes of blue light at 436 nm, inducing the *cis*-to-*trans* isomerization, almost completely restored the G4 levels to their native state (Figure 7A). It is important to note that even if the *cis*-to-*trans* isomerization did not cause the unfolding of

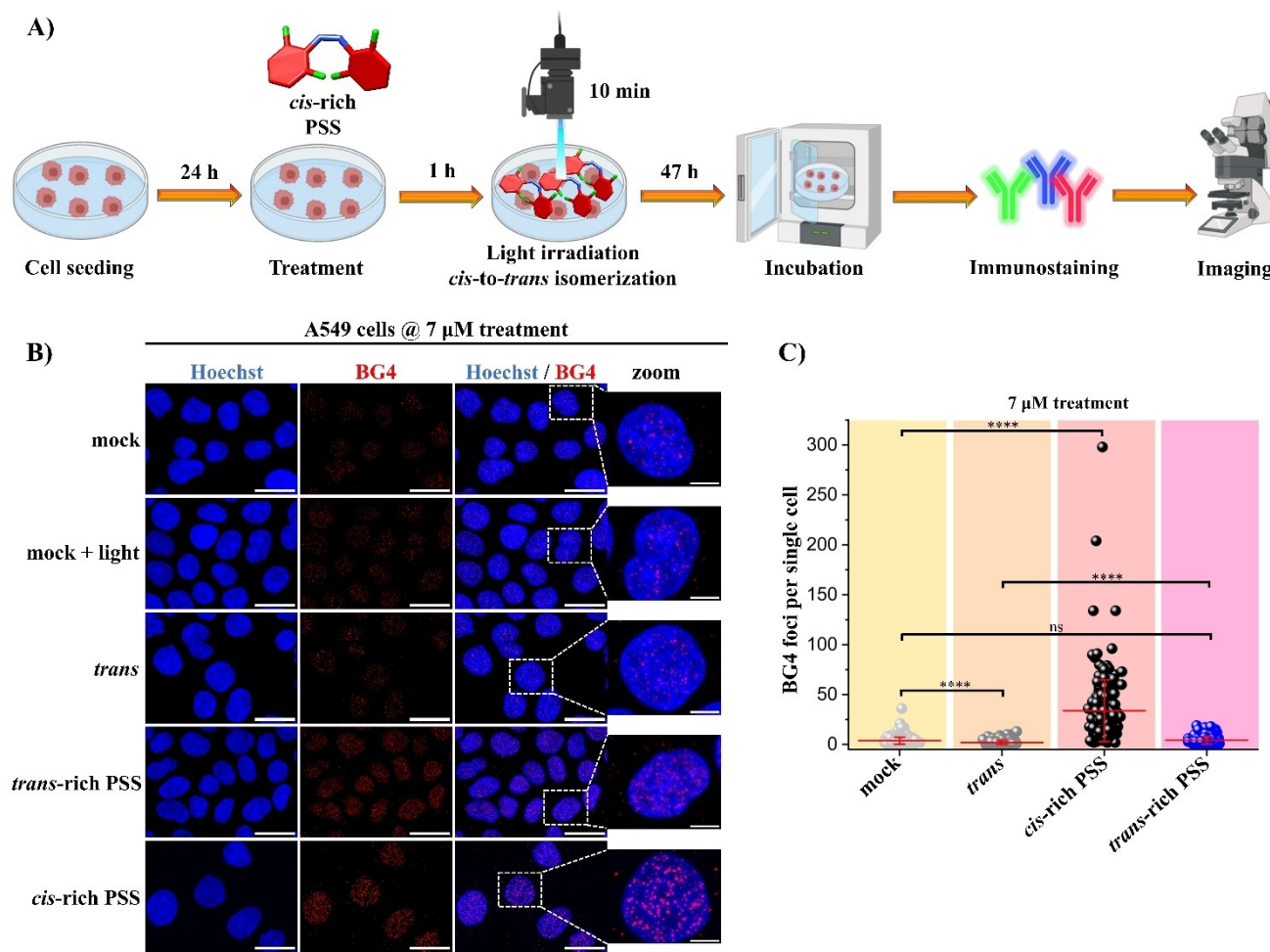


Figure 7. Q-Azo4F-C-mediated photomodulation of G4s in A549 cells. (A) The cells were exposed to a concentration of 7 μ M Q-Azo4F-C in either *trans* or *cis*-rich PSS forms before BG4 immunostaining and imaging. *In-cellulo* photoswitching was accomplished by incubating cells with a 7 μ M concentration of Q-Azo4F-C in its *cis*-rich PSS form for 1 hour followed by 10 minutes exposure of 436 nm blue light. Image created with Biorender.com (B) Immunofluorescence staining of A549 cells treated with a 7 μ M concentration of Q-Azo4F-C in *trans*, *cis*-rich PSS and *trans*-rich PSS, or with equivalent amounts of DMSO. A549 cells were co-stained with the nuclear dye Hoechst 33342 (500 nM, blue). Red foci indicate BG4-mediated G4 recognition. $\lambda_{\text{exc}}/\lambda_{\text{em}}$: 405/420–460 nm for Hoechst (blue signal) and 598/620–750 for BG4 (red signal). The scale bar is set at 20 μ m for regular images and 5 μ m for the enlarged images. (C) Quantification of BG4 signal in the nucleus of A549 cells in the experimental conditions provided in B. Data represent populations of individual cells ($N_{\text{mock}} = 279$ cells, $N_{\text{trans}} = 189$ cells, $N_{\text{cis-rich PSS}} = 206$ cells, $N_{\text{trans-rich PSS}} = 141$ cells). The error bars represent mean \pm SD. Data analysis was performed using a two-sample *t*-test, and the significance level is denoted by the asterisks (*****p* < 0.0001). Ns stands for not significant.

the G4s in cells below their basal level, it still has the potential to validate the concept of reversible modulation of G4 landscapes using Q-Azo4F-C. We postulate that the absence of complete reversibility might stem from a partial fraction of the *cis* isomer, which remains irreversibly bound to the G4s, potentially obstructing its nearly quantitative *cis*-to-*trans* isomeric transition.

Conclusions

In summary, we have pioneered the development of a G4-targeted molecular switch, demonstrating an exceptionally efficient and tunable anti-tumor effect through the interaction of G4 structures with different isomeric forms. Q-Azo4F-C can facilitate G4 modulative processes by altering

the switch's geometry using visible light. This research suggests that regulating G4s through light-sensitive compounds is not only a promising strategy for targeting cancer cells, causing significant damage to their genome, particularly in instances where the cells have a compromised DDR machinery. It also holds potential for targeting brain cells in conditions where an overabundance of G4s leads to impaired G4-helicase activity, which may contribute to neurological disorders. At this point, further investigations are warranted to gain a comprehensive understanding of the genome-wide effects of Q-Azo4F-C and its potential influence on biological processes, particularly concerning DNA replication and repair. However, the findings presented in this study represent a novel contribution, potentially paving the way for new molecular concepts that could lead to innovative therapeutic interventions.

Supporting Information

The authors have cited additional references within the Supporting Information.

Author Contributions

Conceptualization (M.Du and M.De), design, synthesis and characterization of the compound (M.Du), photophysical and biophysical studies (M.Du), designed biological studies (M.De), carried out biological experiments and data analysis (M.De and M.Du), supervision of biological studies (M.De and N.S), MD simulation and data analysis (L.L.-P, J.J.N and L.M.-F), writing original draft (M.De with inputs from all authors), review and editing (M.Du with inputs from M.De), funding acquisition (M.Du, M.De and N.S), project administration (M.Du). All authors approved the final version of the manuscript.

Acknowledgements

This work was supported by the National Science Center (NCN, Poland) under the Sonata project No. UMO-2021/43/D/ST4/00997. M. Du. acknowledges financial support from Wrocław University of Science and Technology and Academia Iuvenum. All cellular studies were conducted at Umeå University in N.S laboratory during M.Du.'s short-term internship. M.De. would like to acknowledge financial support from project No. 2022/47/P/NZ5/01156, which is co-funded by the National Science Centre and the European Union's Horizon 2020 research and innovation program under the Marie Skłodowska-Curie grant agreement No. 945339. M.De also thanks the Swedish Cancer Society for providing financial support through the postdoctoral fellowship (21 0302 PT 01 H). We acknowledge the Biochemical Imaging Center (BICU) at Umeå University and the National Microscopy Infrastructure, NMI(VR-RFI 2019-00217) for providing assistance in microscopy, the Chemical Biology Consortium Sweden (CBCS) at Umeå University for access to the Synergy H4 microplate reader, and the Protein Production Sweden (a national research infrastructure funded by the Swedish Research Council) at Umeå University for purification of the BG4 antibody. Work in N. S. lab received support from the Swedish Cancer Society (22 2380 Pj 01 H), the Swedish Research Council (VR-MH 2021-02468), and Knut and Alice Wallenberg foundations (KAW 2021.0173). L.L.-P. acknowledges the FPU22/02196 grant from the Spanish Ministry of Science, Innovation and Universities (MICINN). J.J.N. acknowledges the financial support from the Comunidad de Madrid through the Attraction of Talent Program (Grant reference 2022-5A/BMD-24244) and the Spanish Ministry of Science and Innovation (MCIN/AEI/10.13039/501100011033) through the project PID2022-138470NB-I00.

Conflict of Interest

The authors declare no conflict of interest.

Data Availability Statement

The data that support the findings of this study are available in the supplementary material of this article.

Keywords: Azobenzene • Cancer cells • DNA • G-quadruplex • Photochromism

- [1] a) N. Kosiol, S. Juranek, P. Brossart, A. Heine, K. Paeschke, *Molecular Cancer* **2021**, 20, 40; b) S. Neidle, *J. Med. Chem.* **2016**, 59, 5987–6011; c) S. Neidle, *Nat. Chem. Rev.* **2017**, 1, 0041.
- [2] a) G. Biffi, D. Tannahill, J. McCafferty, S. Balasubramanian, *Nat. Chem.* **2013**, 5, 182–186; b) S. A. Johnson, T. Paul, S. L. Sanford, B. L. Schnable, A. C. Detwiler, S. A. Thosar, B. Van Houten, S. Myong, P. L. Opresko, *Nucleic Acids Res.* **2023**, 52, 1763–1778; c) G. Biffi, D. Tannahill, J. Miller, W. J. Howat, S. Balasubramanian, *PLoS One* **2014**, 9, e102711; d) J. Spiegel, S. Adhikari, S. Balasubramanian, *Trends Chem.* **2020**, 2, 123–136; e) G. Wang, K. M. Vasquez, *Nat. Rev. Genet.* **2023**, 24, 211–234.
- [3] a) I. Obi, M. Rentoft, V. Singh, J. Jamroskovic, K. Chand, E. Chorell, F. Westerlund, N. Sabouri, *Nucleic Acids Res.* **2020**, 48, 10998–11015; b) C. S. Casas-Delucchi, M. Daza-Martin, S. L. Williams, G. Coster, *Nat. Commun.* **2022**, 13, 3953; c) D. Schiavone, S. K. Jozwiakowski, M. Romanello, G. Guilbaud, T. A. Guillian, L. J. Bailey, J. E. Sale, A. J. Doherty, *Mol. Cell* **2016**, 61, 161–169; d) D. Dahan, I. Tsirkas, D. Dovrat, M. A. Sparks, S. P. Singh, R. Galletto, A. Aharoni, *Nucleic Acids Res.* **2018**, 46, 11847–11857; e) M. A. Sparks, S. P. Singh, P. M. Burgers, R. Galletto, *Nucleic Acids Res.* **2019**, 47, 8595–8605; f) M. Varon, D. Dovrat, J. Heuzé, I. Tsirkas, S. P. Singh, P. Pasero, R. Galletto, A. Aharoni, *Nucleic Acids Res.* **2023**, 52, 1753–1762.
- [4] a) J. Jamroskovic, M. Doimo, K. Chand, I. Obi, R. Kumar, K. Brännström, M. Hedenström, R. Nath Das, A. Akhunzianov, M. Deiana, K. Kasho, S. Sulis Sato, P. L. Pourbozorgi, J. E. Mason, P. Medini, D. Öhlund, S. Wanrooij, E. Chorell, N. Sabouri, *J. Am. Chem. Soc.* **2020**, 142, 2876–2888; b) H. Xu, M. Di Antonio, S. McKinney, V. Mathew, B. Ho, N. J. O'Neil, N. D. Santos, J. Silvester, V. Wei, J. Garcia, F. Kabeer, D. Lai, P. Soriano, J. Banáth, D. S. Chiu, D. Yap, D. D. Le, F. B. Ye, A. Zhang, K. Thu, J. Soong, S.-C. Lin, A. H. C. Tsai, T. Osako, T. Algara, D. N. Saunders, J. Wong, J. Xian, M. B. Bally, J. D. Brenton, G. W. Brown, S. P. Shah, D. Cescon, T. W. Mak, C. Caldas, P. C. Stirling, P. Hieter, S. Balasubramanian, S. Aparicio, *Nat. Commun.* **2017**, 8, 14432; c) R. Rodriguez, K. M. Miller, J. V. Forment, C. R. Bradshaw, M. Nikan, S. Britton, T. Oelschlaegel, B. Xhemalce, S. Balasubramanian, S. P. Jackson, *Nat. Chem. Biol.* **2012**, 8, 301–310.
- [5] a) M. Deiana, J. M. Andrés Castán, P. Josse, A. Kahsay, D. P. Sánchez, K. Morice, N. Gillet, R. Ravindranath, A. K. Patel, P. Sengupta, I. Obi, E. Rodriguez-Marquez, L. Khrouz, E. Dumont, L. Abad Galán, M. Allain, B. Walker, H. S. Ahn, O. Maury, P. Blanchard, T. Le Bahers, D. Öhlund, J. von Hofsten, C. Monnerneau, C. Cabanetos, N. Sabouri, *Nucleic Acids Res.* **2023**, 51, 6264–6285; b) W. Chen, Y. Zhang, H.-B. Yi, F. Wang, X. Chu, J.-H. Jiang, *Angew. Chem. Int. Ed.* **2023**, 62, e202300162; c) T. Gustavsson, D. Markovitsi, *Acc. Chem. Res.*

- 2021, 54, 1226–1235; d) E. Balanikas, A. Banyasz, T. Douki, G. Baldacchino, D. Markovitsi, *Acc. Chem. Res.* **2020**, 53, 1511–1519; e) L. Martínez-Fernández, L. Esposito, R. Imprata, *Photochem. Photobiol. Sci.* **2020**, 19, 436–444.
- [6] A. M. Fleming, C. J. Burrows, *J. Am. Chem. Soc.* **2020**, 142, 1115–1136.
- [7] a) J. Ramos-Soriano, M. C. Galan, *JACS Au* **2021**, 1, 1516–1526; b) X. Wang, J. Huang, Y. Zhou, S. Yan, X. Weng, X. Wu, M. Deng, X. Zhou, **2010**, 49, 5305–5309; c) X. Xing, X. Wang, L. Xu, Y. Tai, L. Dai, X. Zheng, W. Mao, X. Xu, X. Zhou, *Org. Biomol. Chem.* **2011**, 9, 6639–6645; d) M. Dudek, M. Deiana, Z. Pokladek, P. Mlynarz, M. Samoc, K. Matczyszyn, *Nanoscale* **2018**, 10, 11302–11306; e) T. Tian, Y. Song, J. Wang, B. Fu, Z. He, X. Xu, A. Li, X. Zhou, S. Wang, X. Zhou, *J. Am. Chem. Soc.* **2016**, 138, 955–961; f) M. Dudek, M. Deiana, K. Szkaradek, M. J. Janicki, Z. Pokladek, R. W. Góra, K. Matczyszyn, *J. Phys. Chem. Lett.* **2021**, 12, 9436–9441; g) M. Deiana, M. Mosser, T. Le Bahers, E. Dumont, M. Dudek, S. Denis-Quanquin, N. Sabouri, C. Andraud, K. Matczyszyn, C. Monnereau, L. Guy, *Nanoscale* **2021**, 13, 13795–13808.
- [8] a) P. Kobauri, F. J. Dekker, W. Szymanski, B. L. Feringa, **2023**, 62, e202300681; b) I. M. Welleman, M. W. H. Hoorens, B. L. Feringa, H. H. Boersma, W. Szymański, *Chem. Sci.* **2020**, 11, 11672–11691.
- [9] P. Murat, M. V. Gormally, D. Sanders, M. D. Antonio, S. Balasubramanian, *Chem. Commun.* **2013**, 49, 8453–8455.
- [10] T. Kench, P. A. Summers, M. K. Kuimova, J. E. M. Lewis, R. Vilar, *Angew. Chem. Int. Ed.* **2021**, 60, 10928–10934.
- [11] a) M. P. O'Hagan, S. Haldar, M. Duchi, T. A. A. Oliver, A. J. Mulholland, J. C. Morales, M. C. Galan, *Angew. Chem. Int. Ed.* **2019**, 58, 4334–4338; b) M. P. O'Hagan, S. Haldar, J. C. Morales, A. J. Mulholland, M. C. Galan, *Chem. Sci.* **2021**, 12, 1415–1426.
- [12] T. Tian, Y. Song, L. Wei, J. Wang, B. Fu, Z. He, X.-R. Yang, F. Wu, G. Xu, S.-M. Liu, C. Li, S. Wang, X. Zhou, *Nucleic Acids Res.* **2017**, 45, 2283–2293.
- [13] D. Bléger, J. Schwarz, A. M. Brouwer, S. Hecht, *J. Am. Chem. Soc.* **2012**, 134, 20597–20600.
- [14] a) A. Ghosh, M. Trajkovski, M.-P. Teulade-Fichou, V. Gabelica, J. Plavec, *Angew. Chem. Int. Ed.* **2022**, 61, e202207384; b) M. Deiana, J. Jamroskovic, I. Obi, N. Sabouri, *Chem. Commun.* **2020**, 56, 14251–14254; c) B. Prasad, M. Doimo, M. Andréasson, V. L'Hôte, E. Chorell, S. Wanrooij, *Chem. Sci.* **2022**, 13, 2347–2354.
- [15] L.-Y. Liu, T.-Z. Ma, Y.-L. Zeng, W. Liu, Z.-W. Mao, *J. Am. Chem. Soc.* **2022**, 144, 11878–11887.
- [16] a) H. Sun, J. Xiang, Y. Liu, L. Li, Q. Li, G. Xu, Y. Tang, *Biochimie* **2011**, 93, 1351–1356; b) P. Lejault, J. Mitteaux, F. R. Sperti, D. Monchaud, *Cell Chem. Biol.* **2021**, 28, 436–455.
- [17] D. R. Calabrese, X. Chen, E. C. Leon, S. M. Gaikwad, Z. Phyto, W. M. Hewitt, S. Alden, T. A. Hilimire, F. He, A. M. Michalowski, J. K. Simmons, L. B. Saunders, S. Zhang, D. Connors, K. J. Walters, B. A. Mock, J. S. Schneekloth, *Nat. Commun.* **2018**, 9, 4229.
- [18] M. Andréasson, N. Bhuma, N. Pemberton, E. Chorell, *Chem. Eur. J.* **2022**, 28, e202202020.
- [19] a) M. Deiana, I. Obi, M. Andreasson, S. Tamilselvi, K. Chand, E. Chorell, N. Sabouri, *ACS Chem. Biol.* **2021**, 16, 1365–1376; b) M. Deiana, K. Chand, J. Jamroskovic, R. N. Das, I. Obi, E. Chorell, N. Sabouri, *Nanoscale* **2020**, 12, 12950–12957; c) J. Dai, M. Carver, L. H. Hurley, D. Yang, *J. Am. Chem. Soc.* **2011**, 133, 17673–17680.
- [20] A. Ambrus, D. Chen, J. Dai, R. A. Jones, D. Yang, *Biochemistry* **2005**, 44, 2048–2058.
- [21] A. V. Melkikh, M. I. Sutormina, *J. Theor. Biol.* **2008**, 252, 247–254.
- [22] M. Hafner, M. Niepel, M. Chung, P. K. Sorger, *Nat. Methods* **2016**, 13, 521–527.
- [23] a) F. Raguseo, Y. Wang, J. Li, M. Petrić Howe, R. Balendra, A. Huyghebaert, D. M. Vadukul, D. A. Tanase, T. E. Maher, L. Malouf, R. Rubio-Sánchez, F. A. Aprile, Y. Elani, R. Patani, L. Di Michele, M. Di Antonio, *Nat. Commun.* **2023**, 14, 8272; b) J. Mitteaux, P. Lejault, F. Wojciechowski, A. Joubert, J. Boudon, N. Desbois, C. P. Gros, R. H. E. Hudson, J.-B. Boulé, A. Granzhan, D. Monchaud, *J. Am. Chem. Soc.* **2021**, 143, 12567–12577.
- [24] J. Mitteaux, S. Raevens, Z. Wang, M. Pirrotta, I. E. Valverde, R. H. E. Hudson, D. Monchaud, *Chem. Commun.* **2024**.
- [25] M. Dudek, L. López-Pacios, N. Sabouri, J. J. Nogueira, L. Martinez-Fernandez, M. Deiana, *J. Phys. Chem. Lett.* **2024**, 38, 9757–9765. <https://doi.org/10.1021/acs.jpclett.4c02285>

Manuscript received: July 10, 2024

Accepted manuscript online: September 13, 2024

Version of record online: November 6, 2024